Am J Physiol Heart Circ Physiol 308: H733–H742, 2015.
First published January 23, 2015; doi:10.1152/ajpheart.00335.2014.

The impact of capillary dilation on the distribution of red blood cells in artificial networks

Franca Schmid,[1] Johannes Reichold,[1] Bruno Weber,[2] and Patrick Jenny[1]

[1]*Institute of Fluid Dynamics, ETH Zurich, Zurich, Switzerland; and* [2]*Institute of Pharmacology and Toxicology, University of Zurich, Zurich, Switzerland*

Submitted 19 May 2014; accepted in final form 21 January 2015

Schmid F, Reichold J, Weber B, Jenny P. The impact of capillary dilation on the distribution of red blood cells in artificial networks. *Am J Physiol Heart Circ Physiol* 308: H733–H742, 2015. First published Janaury 23, 2015; doi:10.1152/ajpheart.00335.2014.—Recent studies suggest that pericytes around capillaries are contractile and able to alter the diameter of capillaries. To investigate the effects of capillary dilation on network dynamics, we performed simulations in artificial capillary networks of different sizes and complexities. The unequal partition of hematocrit at diverging bifurcations was modeled by assuming that each red blood cell (RBC) enters the branch with the faster instantaneous flow. Network simulations with and without RBCs were performed to investigate the effect of local dilations. The results showed that the increase in flow rate due to capillary dilation was less when the effects of RBCs are included. For bifurcations with sufficient RBCs in the parent vessel and nearly equal flows in the branches, the flow rate in the dilated branch did not increase. Instead, a self-regulation of flow was observed due to accumulation of RBCs in the dilated capillary. A parametric study was performed to examine the dependence on initial capillary diameter, dilation factor, and tube hematocrit. Furthermore, the conditions needed for an efficient self-regulation mechanism are discussed. The results support the hypothesis that RBCs play a significant role for the fluid dynamics in capillary networks and that it is crucial to consider the blood flow rate and the distribution of RBCs to understand the supply of oxygen in the vasculature. Furthermore, our results suggest that capillary dilation/constriction offers the potential of being an efficient mechanism to alter the distribution of RBCs locally and hence could be important for the local regulation of oxygen delivery.

capillary dilation; red blood cells; RBCs; neurovascular coupling; cortical capillary network; numerical model

A PROFOUND UNDERSTANDING OF flow in vascular networks is the basis for a wide range of research topics related to energy metabolism. In the case of the brain, it is known that increases in neuronal activity coincide with a marked increase in local energy demand and that local vascular changes occur to rapidly upregulate oxygen and glucose delivery. Recent evidence has shown that pericytes are contractile cells capable of locally changing the cross sections of capillaries (25, 36). In contrast to networks in other organs, the cerebral vasculature shows significant pressure gradients across capillaries (4). Thus, from a physiological and fluid dynamical view point, flow regulation at the capillary level is feasible and effective. However, several fundamental questions related to capillary regulation remain open. For example, *1*) how local and how large is the influence of dilation/constriction on flow and hematocrit, *2*) how are transit times affected, and *3*) what is the relevance for cerebral blood flow regulation or for any other organs.

Addressing these topics experimentally is difficult because multiple capillaries have to be monitored at the same time. However, various works in the rat cerebral cortex recorded changes in red blood cell (RBC) velocity, RBC distribution, and RBC supply rate induced by electrical stimulation (46) or by hypercapnia (52). The results of both works point towards further mechanisms, besides the increased RBC supply rate resulting from arteriole dilation, which alter the distribution of RBCs to locally upregulate oxygen supply. Dilation of one or multiple capillaries could explain the observed phenomena.

Numerical simulations so far have focused on reproducing the hematocrit distribution (43, 45, 47) and on defining appropriate boundary conditions for realistic networks (24, 32). A further area of research is the dynamics of microvascular networks with and without white blood cells (11, 19, 23, 28). Reichold et al. (44) investigated the effects of arteriole dilation on cerebral blood flow. However, the model introduced by Reichold et al. is not suitable to study the distribution of RBCs as the tube hematocrit is only a function of vessel diameter and hence is constant for one network topology. Lorthois and Lauwers (34) simulated dilations of either all or a randomly chosen set of capillaries. However, to our knowledge no systematic study focusing on single capillary dilation exists.

As early as 1972, Fung (22) considered flow in a bifurcation with two branches of equal diameter and noted that the tendency of RBCs to enter the branch with faster flow would increase the flow resistance in that branch, thereby reducing the flow in that branch. This phenomenon, which we term self-regulation (SR), has the effect of reducing the disparity between the flow rates in the downstream branches of a diverging bifurcation. Therefore, we expect that in statistical steady state and within the limitations of SR the outflow velocities and flow rates are equalized. The self-regulating behavior has also been observed by Furman and Olbricht (23) and Sessoms et al. (49).

The phase-separation effect and the discrete nature of RBCs lead to spatial and temporal fluctuations in the RBC velocity and the RBC distribution throughout the capillary network. Many experimental studies focused on quantifying the variations in RBC velocity and tube hematocrit (15, 16, 27, 29, 47, 51). In further studies, the fluctuations in single capillaries have been quantified (13, 14). Those results underline the importance of taking into account the RBC-induced SR based on the interdependence of RBCs and blood flow to fully understand the flow in the microcirculation. Despite its importance for fluid dynamics in capillary networks, only a few numerical investigations addressed the topic of SR in larger microvascular networks (35, 38).

Address for reprint requests and other correspondence: F. Schmid, Institute of Fluid Dynamics, ETH Zurich, Zurich, Switzerland (e-mail: schmid@ifd.mavt.ethz.ch).

 0363-6135/15 Copyright © 2015 the American Physiological Society

Downloaded from journals.physiology.org/journal/ajpheart (192.041.132.005) on June 11, 2024.

In the present study, simplified capillary networks are analyzed with several objectives in mind: *1*) to quantify the effects of capillary dilation and comment on its role in neurovascular coupling, *2*) to point out that both the RBC distribution and the RBC supply rate need to be considered to understand the oxygen supply mechanisms in the vasculature, and *3*) to systematically study the impact of RBCs on the flow in the microcirculation and underline the importance of treating blood as a biphasic fluid.

The first step consists of investigating effects of local dilations in the presence and absence of RBCs. The resulting RBC concentrations and blood flow distributions were compared. Furthermore, we analyzed the flow separation at divergent bifurcations throughout the network for simulations with and without RBCs.

The applied simulation model is based on the discrete RBC model presented by Obrist et al. (35), which differs significantly from other models, where the RBC flow is calculated by empirically derived equations. In the empirically derived models, the steady-state solution is obtained by an iterative approach, which considers the phase-separation effect at divergent bifurcations by applying an empirically derived function (47). For the phase-separation effect, various empirical functions have been used in different works (11, 24, 41, 47). The formulation by Pries and Secomb (41) and Pries et al. (43) is one of the most widely used functions.

Guibert et al. (24) studied the impact of different phase-separation laws on the hematocrit distribution in realistic networks. They concluded that the applied phase separation law has a relatively small effect on the pressure distribution but a strong effect on the hematocrit distribution. The empirical model has been used to study flow in different systemic tissues, such as the rat mesentry (47) and the cerebral vasculature (24, 32, 33, 34).

The discrete approach was first used as by Schmid-Schönbein et al. (45) and Furman and Olbricht (23). Both studies report for diverging bifurcations that RBCs favor the branch with the larger flow rate. This is in contrast to our approach, where the RBCs follow the path of the largest bulk flow velocity, as stated by Fung (22) and Yen and Fung (53). In previous work by Fenton et al. (19) and by Pozrikidis (38) particles are also tracked, but at divergent bifurcations an empirically derived function was used to describe the movement of RBCs. Further approaches use the convection equation to compute the hematocrit distribution (8, 37) or groups of RBCs (="slugs") are followed individually (28).

Hence, our work is the first which studies the distribution of RBCs and the effects of capillary dilation in larger artificial networks, where the phase separation effect is modeled by assuming that each RBC enters the branch with the larger instantaneous flow.

DISCRETE RBC MODEL FOR CAPILLARY NETWORKS

To systematically study flow and RBC transport at the capillary level, simplified yet representative networks are considered, which are described in *Simplified Capillary Networks*. The flow equations and the simulation procedure are presented in *Governing Equations* and *Simulation Procedure*.

Simplified Capillary Networks

The capillary networks used for the simulation studies in this article are approximated by straight tubes, each connecting two nodes (Fig. 1). A node can either be a bifurcation with three adjacent tubes or an inner node connecting two tube segments. The latter case is relevant, since only dilations of inner vessel segments (between 2 inner nodes) are considered (Fig. 1*A*). Initially the diameters of all tubes are identical (baseline). In case of dilation, the diameter of an inner segment is increased by the dilation factor f_{Dil}; note that the segments adjacent to divergent bifurcations remain unaltered.

Further simplifications compared with real vascular networks are that tortuosity and cross sectional variations are not taken into account.

Governing Equations

For a pipe with diameter D, the Reynolds number is defined as $Re = \rho u D/\mu$, where u is the bulk flow velocity, ρ the fluid density, and μ the dynamic viscosity of the fluid. Due to very small Reynolds numbers in the microcirculation ($Re < 0.1$), inertial effects can be neglected. Therefore, the Navier-Stokes equation reduces to the Stokes equation

$$\mu \nabla^2 u - \nabla p = 0, \tag{1}$$

where p is the pressure. Furthermore, the fluid can be considered incompressible and therefore the continuity equation reads

$$\nabla \cdot u = 0. \tag{2}$$

From *Eq. 1* it can be derived that the flow rate in a tube connecting nodes i and j can be calculated as

$$q_{ij} = \frac{p_i - p_j}{R_{ij}}, \tag{3}$$

where p_i and p_j are the pressure values at the nodes i and j, respectively. R_{ij} is the nominal resistance of the tube connecting the two nodes and is defined as the product of the specific resistance r_{ij} and the

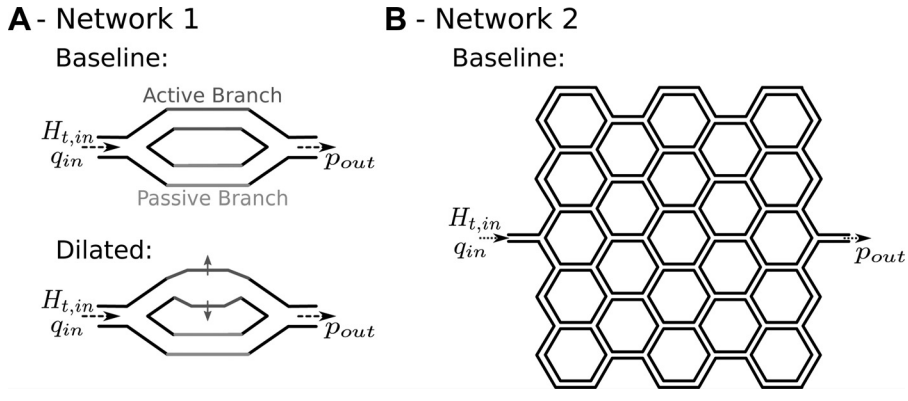

Fig. 1. Artificial networks used to investigate the effects of capillary dilation. For *network 1* (*A*), the baseline and the dilated case are illustrated. *B*: *network 2*. $H_{\mathrm{t,in}}$, inflow tube hematocrit; q_{in}, inflow rate; p_{out}, outlet pressure.

Downloaded from journals.physiology.org/journal/ajpheart (192.041.132.005) on June 11, 2024.

length of the tube L_{ij}, i.e., $R_{ij} = r_{ij}L_{ij}$. In agreement with Poiseuille's law for circular tube cross sections and Newtonian fluids, including pure blood plasma, the specific resistance r_{ij} is

$$r_{ij} = \frac{128\mu}{\pi D_{ij}^4}. \quad (4)$$

Note that noncircular cross sections can be considered by a scaling factor. However, blood is a non-Newtonian fluid. The RBC concentration and the diameter of the tube contribute significantly to the effective tube resistance. Here, in line with Ref. 40, the relative apparent viscosity μ_{vitro} is introduced and reads

$$\mu_{vitro} = 1 + (\mu_{0.45} - 1)\frac{(1 - H_d)^C - 1}{(1 - 0.45)^C - 1} \quad (5)$$

$$\text{with } \mu_{0.45} = -220e^{-1.3\,D} + 3.2 - 2.44e^{-0.06\,D^{0.645}} \quad (6)$$

$$\text{and } C = (0.8 + e^{-0.075\,D})\left(-1 + \frac{1}{1 + 10^{-11}D^{12}}\right) + \frac{1}{1 + 10^{-11}D^{-12}} \quad (7)$$

where H_d is the discharge hematocrit. The empirical relation (*Eq. 5*) also accounts for the Fåhraeus-Lindqvist effect, which states that the viscosity of blood strongly depends on the vessel diameter and the hematocrit. According to Fåhraeus and Lindqvist (18), the viscosity of blood decreases with decreasing vessel diameter (up to a point close to 5 μm, below which it increases steeply). Significant discrepancies between in vitro and in vivo measurements of relative apparent viscosity were found by Lipowsky et al. (31). Pries and Secomb (41) attributed those differences to the influence of the endothelial surface layer (ESL) and introduced the relative effective viscosity

$$\mu_{vivo} = \mu_{vitro}\left(\frac{D}{D_{eff}}\right)^4 \quad (8)$$

to account for the ESL. The effective diameter is denoted by D_{eff} and can be computed from the vessel diameter and the effective thickness W_{eff} of the endothelial surface layer (41). Subsequently, the effective resistance of the capillary is equal to $R_{ij}^e = \mu_{vivo}R_{ij}$ and the flow of the suspension between two neighboring vertices can be computed as

$$q_{ij} = \frac{p_i - p_j}{R_{ij}^e}. \quad (9)$$

According to the Fåhraeus effect (17), on average the RBCs travel faster than the bulk flow. This is a consequence of the parabolic flow profile in pipes and the fact that the RBCs are forced to travel on the centerline of the capillary. The different velocities of the bulk flow and the RBCs result in different volume fractions of the RBCs in suspension (discharge hematocrit H_d) and in the vessel (tube hematocrit H_t). Thus the velocity of the RBCs can be obtained from the ratio

$$u_{RBC} = \frac{H_d}{H_t}u_{ij} \quad (10)$$

where tube hematocrit H_t and bulk flow velocity u_{ij} are defined as

$$H_t = \frac{N_{RBC}V_{RBC}}{V} \quad (11)$$

$$\text{and } u_{ij} = \frac{q_{ij}}{A_{ij}}. \quad (12)$$

The number of RBCs is denoted by N_{RBC}; V_{RBC} and V denote RBC and vessel volumes, respectively, and A is the cross-sectional area of the vessel. V_{RBC} is set to 56.51 fl (rat) (3) and kept constant throughout the simulation.

Pries and Secomb (41) derived an empirically based function to calculate the ratio between in vivo tube and discharge hematocrit values as

$$H_t = H_d\left[H_d + (1 - H_d)(1 + 1.7e^{-0.415\,D} - 0.6e^{-0.011\,D})\right]\left(\frac{D}{D_{ph}}\right)^{-2} \quad (13)$$

where D_{ph} is the physical diameter, accounting for the diameter reduction due to the endothelial surface layer (41). The discharge hematocrit H_d is needed to calculate the RBC velocity (*Eq. 10*) and the relative apparent viscosity (*Eq. 5*).

At divergent bifurcations (nodes with 1 inflow and 2 outflow tubes), a rule to track the RBCs is required. It is well established that the ratio of RBC concentrations in the outflow branches is not proportional to the ratio of flow rates (phase-separation effect) and identifying the important factors for this phase-separation effect is subject of ongoing research (1, 2, 10, 12, 39). Respective investigations range from in vivo (39) and in vitro (10, 12) experiments to complex numerical simulations including the deformation of RBCs (2).

To conduct representative blood flow simulations in capillary networks, where each RBC is represented by a computational particle, we need a bifurcation rule that describes the instantaneous RBC movements. In most of the existing numerical works, the empirical function by Pries and colleagues is applied (24, 32, 33, 34, 47). However, this is a description of the time-averaged behavior of RBCs at divergent bifurcations and not of their instantaneous movement. In previous work by Fung (22) and Yen and Fung (53), the RBC moves into the daughter vessel with the larger bulk flow velocity. On the other hand, Schmid-Schönbein et al. (45) and Furman and Olbricht (23) applied a bifurcation criterion which is based on the flow rate. To avoid that our results depend on the chosen bifurcation rule we keep the diameters of all vessels at the bifurcations constant. For such bifurcations, the RBC moves in the same downstream branch for the bulk flow velocity based and the flow rate based bifurcation rule.

The movement of RBCs is implemented such that they may get blocked by others at bifurcations. For example, if two RBCs arrive simultaneously at a convergent bifurcation, one of them has to wait for sufficient space. Moreover, further RBCs might accumulate behind the blocked RBC.

Simulation Procedure

Mass balance at every node i leads to

$$\sum_j q_{ij} = \sum_j \frac{p_i - p_j}{R_{ij}^e} = q_i \quad (14)$$

where q_i is a source term describing flow in and out of the network. If the in- and outflow boundary conditions and the hematocrit in every vessel are known, the flow problem is well defined and can be transformed into a system of linear equations, i.e.

$$\underline{q} = \underline{\underline{N}} \cdot \underline{p}, \quad (15)$$

where the known vector $\underline{q}$ contains the in- and outflow rates and the unknown vector $\underline{p}$ contains the pressure values at each node. The matrix $\underline{\underline{N}}$ results from *Eq. 14*. The simulation procedure can be summarized as follows:

1) Define the network geometry and boundary conditions.

2) Random initialization of RBC positions considering initial tube hematocrit.

3) Calculate effective resistance.

4) Compute pressure and flow field based on *Eq. 14*.

5) Evolve RBCs (*Eq. 10*) until one of them reaches a bifurcation or a blocked RBC.

Downloaded from journals.physiology.org/journal/ajpheart (192.041.132.005) on June 11, 2024.

6) Apply bifurcation rule if necessary.
7) Go to *step 3*.

Due to the bifurcation rule and the impact of the RBCs on the effective resistance we observe oscillations throughout the network. The oscillating behavior has been reported and investigated earlier in various works (7, 8, 11, 19, 23, 28, 38). In the presented work we limit ourselves to analyzing the results for the statistical steady state and do not focus on the oscillations. However, we want to point out that our model is capable of capturing transient changes.

RESULTS

To demonstrate the effects of capillary dilation two simplified capillary networks were used (Fig. 1). We started by analyzing a simple two-branch network (Fig. 1*A*, *network 1*), which consists of one active (capillary dilation) and one passive branch (no capillary dilation). The length of each branch is equal to 150 μm.

The size of the network was increased by assembling two-branch networks to obtain a hexagonal network (Fig. 1*B*, *network 2*). The hexagonal network represents a simplified mesh-like structure as it is found in the cerebral capillary bed (26). In *network 2* the initial diameter of every vessel is equal to 7 μm and the length of each vessel segment was set to 60 μm. The vessel length was chosen based on the work by Secomb et al. (48), who showed that in vessels with a diameter of 8 μm RBCs migrate in the lateral direction and reach a position close to the centerline after a distance of ~60 μm.

The pressure at the outlet was set to $p_{out} = 0$ mmHg. For better comparison the same inflow rate q_{in} was assigned to every network type. It was chosen such that the velocity of the RBCs is in the range of the measured values in the capillary bed. For all cases the focus lies on SR in the case of capillary dilation, its consequences for the distribution of the RBCs, and its limitations.

Two-Branch Network

Network 1 (Fig. 1*A*) was used to illustrate and study SR in the simplest configuration possible. Furthermore, the influence of different parameters (e.g., dilation factor, tube hematocrit) can be analyzed easily and the changes resulting from capillary dilation can be quantified.

The network consists of an active and a passive branch. In the baseline case (without dilation), the bulk flow velocities in the outflow branches of the divergent bifurcation are equal due to the symmetry of the network. To unbalance the system, the diameter in an interior segment of the active branch with a length of 40 μm (total branch length 150 μm) is increased by the dilation factor f_{Dil}, that is,

$$D_{Dil} = (1 + f_{Dil})D_{init}, \quad (16)$$

where D_{init} is the initial diameter, which is the same in the active and the passive branch, and D_{Dil} is the diameter after dilation in the active branch. The diameters at the bifurcation remain unaltered (Fig. 1*A*). Due to the dilation the specific resistance is reduced, and hence, instantaneously the flow rate and the bulk flow velocity increase in the active branch. According to the defined bifurcation rule, balanced bulk flow velocities at the bifurcation and an accumulation of RBCs in the active branch should be obtained in the steady state if sufficient RBCs are present. In the case of equal diameters at the bifurcation, balanced bulk flow velocities are equal to balanced local pressure gradients or flow rates.

Figure 2 shows the steady-state results for different initial capillary diameters D_{init} (Fig. 2*A*) and different inflow tube hematocrits $H_{t,in}$ (Fig. 2*B*) To judge on the effectiveness of SR, the flow rates for the simulation with and without RBCs were compared. Figure 2, *row 1*, depicts the flow rate relative to baseline q/q_{base} for the cases without RBCs ($H_{t,in} = 0.0$) and with an inflow tube hematocrit of $H_{t,in} = 0.4$. For simulations with RBCs the relative flow rate in the steady state is ≈1.0, whereas for $H_{t,in} = 0.0$ the flow rate in the active branch increases/decreases in the case of dilation/constriction. This is due to the lack of RBCs to compensate for the changed specific resistance of the active branch. For $H_{t,in} = 0.4$ the number of RBCs in the active branch increases on average by 12% compared with the baseline case. In the passive branch there are on average 6% less RBCs (Fig. 2, *row 2*), and consequently, the outflow rates at the divergent bifurcation are equalized. Figure 2*B*, *row 2*, shows that for low inlet hematocrits the number of RBCs is significantly more reduced in the passive branch to compensate the induced changes in resistance.

The results for different initial diameters (Fig. 2*A*) show that in the two-branch network SR is more pronounced for larger capillary diameters. This can be explained by the constant RBC volume and the same vessel lengths for simulations with different initial diameters. Hence, for vessels with a larger diameter, more RBCs are needed to obtain the same tube hematocrit (*Eq. 11*). Consequently, the larger the capillary diameter the more RBCs are in the network and the better the system is able to adapt to changes.

Figure 2, *row 3*, illustrates the velocity of the RBCs in the dilated part of the active branch and its undilated counterpart in the passive branch. Whereas the velocity of the RBCs in the passive branch remains nearly unchanged, there is a significant velocity reduction in the dilated segment. The velocity reduc-

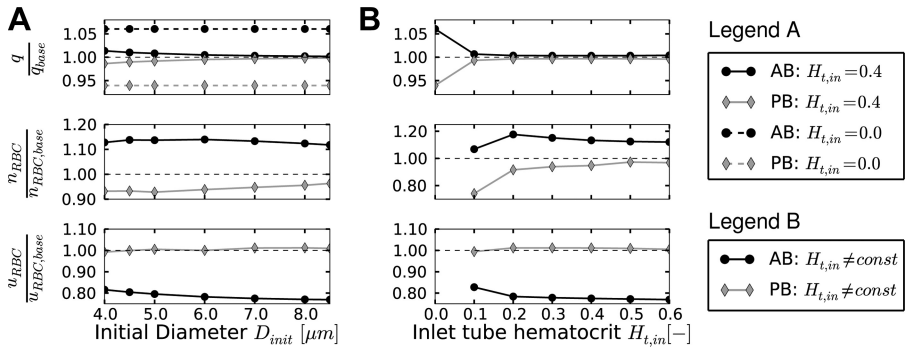

Fig. 2. Averaged flow rate, number of red blood cells (RBCs), and velocity of RBCs relative to the baseline case for different initial diameters (D_{init}; *A*) and different inflow tube hematocrits ($H_{t,in}$; *B*) for the statistical steady state. Black lines illustrate the results in the active branch (AB) and grey lines the ones in the passive branch (PB). For *A*, $f_{Dil} = 15\%$, D_{init} = var., and $H_{t,init}$ = var. For *B*, $f_{Dil} = 15\%$, $D_{init} = 7.0$ μm, and $H_{t,init}$ = var. The n_{RBC} is shown for the whole AB/PB, whereas u_{RBC} is the velocity in the dilated part of the AB and its undilated counterpart in the PB.

Downloaded from journals.physiology.org/journal/ajpheart (192.041.132.005) on June 11, 2024.

tion is due to the diameter change and to smaller extent to the ratio of discharge to tube hematocrit H_d/H_t (*Eq. 10*), which is a function of the vessel diameter.

All simulations support the importance of the RBC-induced SR and underline the necessity to treat blood as a biphasic fluid in capillary networks, because SR is not captured if blood is treated as a single-phase fluid. The parameter study revealed that SR is present in all cases with RBCs but that a higher tube hematocrit in the parent vessel is beneficial for the effectiveness of SR.

Hexagonal Networks

Network 2 (Fig. 1*B*) is used to analyze the effectiveness of SR in larger and more realistic networks. In a first step we analyzed the distribution of RBCs and the flow field for the baseline case. This provides the basis for the investigations on capillary dilation. We continued by comparing baseline cases to networks with dilation, as we did for the two-branch network. As mentioned above, the capillary diameters are the same at the bifurcations; thus, for simplicity, we compare the relative flow rates at the outflow branches of the divergent bifurcation, instead of the bulk flow velocities. The relative flow rate $q_{\mathrm{db,rel}}$ at a divergent bifurcation is defined as the ratio of the flow rate in one of the outflow branches to the flow rate in the inflow branch.

SR for the baseline case. Figure 3 shows the flow rates and the distribution of RBCs for the baseline case in *network 2*. Neither the distribution of flow rates nor the number of RBCs per vessel is homogeneous. The differences in the number of RBCs per vessel are even more pronounced than the differences in flow rate. Whereas there is an accumulation of RBCs close to the axis of symmetry, there is a lack of RBCs in the corners of the network.

To analyze the impact of the RBCs on the network dynamics the relative flow rates at divergent bifurcations are compared for simulations with and without RBCs. In total 23 divergent bifurcations exist in *network 2*. If SR is fully active, the relative flow rate is equal to 0.5 in both outflow branches. To judge on the effectiveness of SR at individual divergent bifurcations the balance factor

$$B_{\mathrm{db},k} = \mathrm{sgn}\left(q_{k,\mathrm{db,rel}} - 0.5\right) \cdot \left(1 - \frac{\left|0.5 - q_{k,\mathrm{db,rel}}\right|}{0.5}\right) \quad (17)$$

for divergent bifurcations is introduced, where $q_{k,\mathrm{db,rel}}$ is one of the two relative flow rates in the divergent branches of bifurcation k. The balance factor $B_{\mathrm{db},k}$ is equal to 1 for perfectly well-balanced bifurcations and equal to 0 for completely ill-balanced bifurcations. The sign of the balance factor is positive for the branch with the higher flow rate and negative for the branch with the lower flow rate.

The averaged balance factor

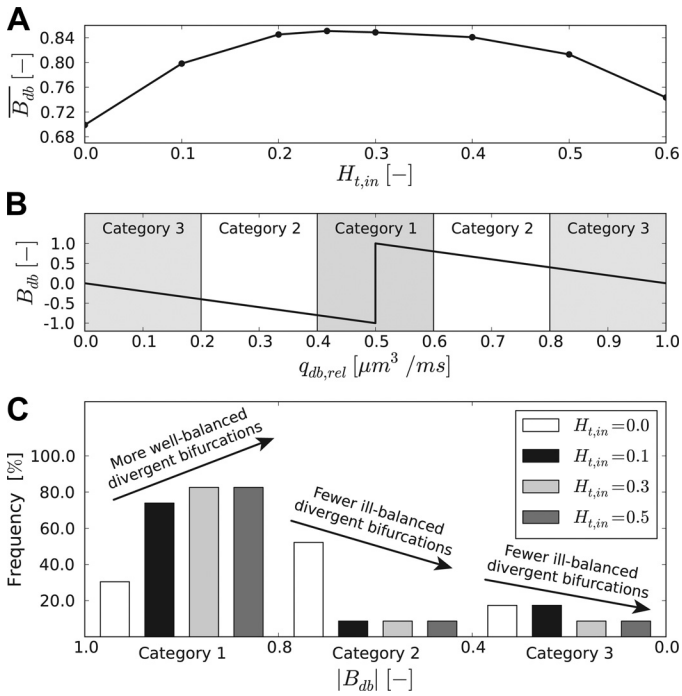

Fig. 4. *A*: averaged balance factor for different $H_{\mathrm{t,in}}$. *B*: balance-factor (B_{db}) for different relative outflow rates at divergent bifurcations ($q_{\mathrm{db,rel}}$). The categories for the histogram are illustrated by different shades. *C*: histogram of the balance factor for different $H_{\mathrm{t,in}}$ in *network 2*. Divergent bifurcations in *category 1* are considered as well balanced.

$$\overline{B_{\mathrm{db}}} = \frac{1}{|J|}\sum_{k\in J}\left|B_{\mathrm{db},k}\right| \text{ where } \mathrm{J}=\left\{i \in M_{\mathrm{div}}\right\} \quad (18)$$

is the network average of the balance factor $B_{\mathrm{db},k}$, where M_{div} is the set of all outflow branches of divergent bifurcations. It is used to compare the overall network balance for different networks and different boundary conditions. The averaged balance factor strongly depends on the network geometry and the inflow tube hematocrit and approaches 1 for networks in equilibrium (balanced outflow rates at every divergent bifurcation). To measure the overall network balance, the averaged balance factor and histograms of the balance factor are used. For the histograms the balance factors are grouped into three bins: *category 1*: $|B_{\mathrm{db}}| > 0.8$; *category 2*: $0.8 \geq |B_{\mathrm{db}}| > 0.4$; and *category 3*: $0.4 \geq |B_{\mathrm{db}}|$. Divergent bifurcations belonging to *category 1* are considered as well balanced.

The overall network balance of *network 2* for different $H_{\mathrm{t,in}}$ is summarized in Fig. 4. The highest averaged balance factor is achieved with $H_{\mathrm{t,in}} = 0.25$ (Fig. 4*A*). If $H_{\mathrm{t,in}}$ is increased further, the averaged balance factor drops again. Also, concerning the number of ill-balanced bifurcations, no improvement can be achieved by increasing $H_{\mathrm{t,in}}$ further (Fig. 4*C*). Thus it is assumed

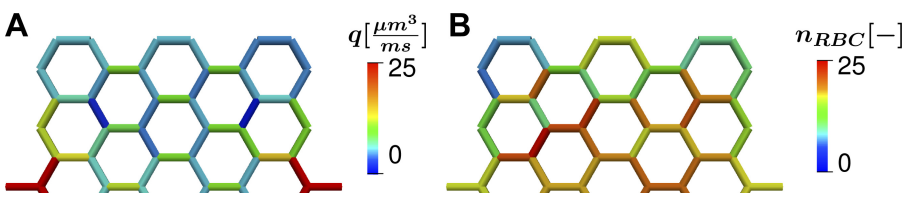

Fig. 3. Flow rate (*A*) and number of RBCs (*B*) for every vessel in *network 2* with $H_{\mathrm{t,in}} = 0.4$. Because of the symmetry, only half of the network is shown.

Downloaded from journals.physiology.org/journal/ajpheart (192.041.132.005) on June 11, 2024.

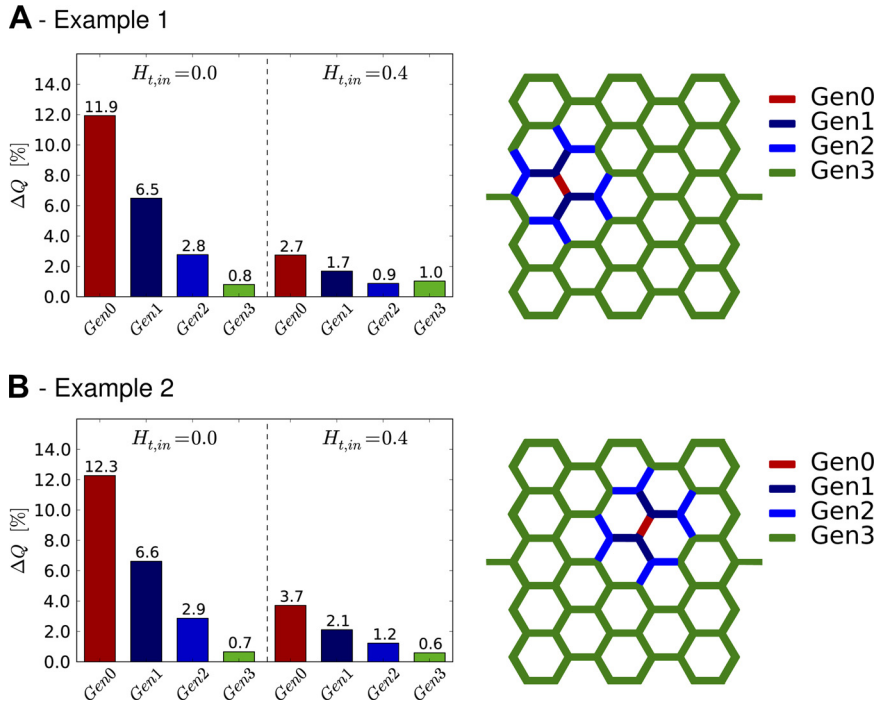

Fig. 5. Averaged relative flow change (ΔQ_{GenX}) for different generations in 2 example cases (*A* and *B*). The results are compared for simulations without RBCs ($H_{t,in} = 0.0$) and with $H_{t,in} = 0.4$. The dilated capillary is highlighted in red in the schematic drawing of *network 2*. $f_{Dil} = 15\%$ for all cases.

that for $H_{t,in} > 0.25$ the effects of RBC blockage become more important and hinder further balancing. For $H_{t,in} < 0.25$ the parent vessel does not contain sufficient RBCs to completely balance the downstream divergent bifurcation. From the results shown in Fig. 4 it can be seen that the presence of RBCs significantly improves the overall network balance. This constitutes a very important property of the network dynamics.

SR in response to capillary dilation. The next step consists of analyzing the effects of capillary dilation in *network 2* and of investigating the factors influencing the effectiveness of the SR. In larger networks not only the changes in the dilated branch itself, but also the influence on the neighboring vessels and the rest of the network are of interest. Therefore the network is divided into different sections and the SR factor SR_{GenX} is introduced. The dilated capillary is considered as *generation 0* capillary (*Gen0*). The direct neighboring vessels are grouped as capillaries of *generation 1* (*Gen1*), and accordingly, their neighbors are capillaries belonging to *generation 2* (*Gen2*). All remaining capillaries in the network are assembled in *generation 3* (*Gen3*). For each generation the averaged relative flow change ΔQ_{GenX} is calculated. It is defined as

$$\Delta Q_{GenX} = \frac{1}{|I|}\sum_{k\in I}\frac{|qk - qk,\text{base}|}{qk,\text{base}} \quad \text{with} \quad I = \{i \in GenX\}, \tag{19}$$

where q_{base} stands for the results of the simulation for the baseline flow and *GenX* is the set of capillaries belonging to *generation X*.

Figure 5 shows the averaged relative flow change ΔQ_{GenX} for *generations 0–3* for two exemplary cases. For all cases the inflow rate was set to $q_{in} = 50$ μm³/ms and the capillary diameter was increased by 15% from 7.0 to 8.05 μm in an inner segment with a length of 48 μm. The total length of the branch is 60 μm, and the diameters at the divergent bifurcations are kept constant. The relative flow change for *Gen0* with RBCs is more than 4.0 times smaller than for simulations without RBCs. The equivalent trend is found for *Gen1*. *Gen2*, and *Gen3* represent the influence on the capillaries, which are not direct neighbors of the dilated capillary. The relative flow change for *Gen2* and *Gen3* depends on the overall network balance, and for *example 1* we observe a slight increase of ΔQ_{Gen3}. As ΔQ_{Gen3} is very low in general, we consider the small increase of ΔQ_{Gen3} as negligible. Therefore, the conclusion that the flow rates in the network are not affected significantly by capillary dilation at well-balanced bifurcations holds true. The accumulation of RBCs, the velocity reduction, and the increased RBC flow rate in the dilated branch observed in *network 1* are confirmed by the results for *network 2* (Table 1). Due to the reduced flow velocity the averaged RBC transit time for RBCs passing through the dilated branch increased by 5% and by 1% for *examples 1* and *2*, respectively. To study the impact of capillary dilation on RBC transit time in more detail, realistic networks should be used and the RBC path should be recorded. One possible explanation for the smaller increase of RBC transit time in *example 2* is that the dilated capillary is located further downstream and hence its impact on the transit time is smaller.

Importantly, not every divergent bifurcation in *network 2* is perfectly well balanced for the baseline case, and consequently, the flow conditions at individual divergent bifurcations differ significantly. It seems likely that the flow separation influences

Table 1. *Number of RBCs, RBC velocity, and RBC flow rate for the 2 examples shown in Fig. 5*

	n_{RBC}		u_{RBC}, mm/s		q_{RBC}, l/s	
Example	Baseline	Dilated	Baseline	Dilated	Baseline	Dilated
1	17.9	23.4	0.24	0.19	49.3	77.6
2	17.8	23.0	0.38	0.30	37.6	59.9

The results are compared for the baseline and the dilated cases. n_{RBC}, number of red blood cells (RBCs); u_{RBC}, RBC velocity; q_{RBC}, RBC flow rate.

Downloaded from journals.physiology.org/journal/ajpheart (192.041.132.005) on June 11, 2024.

the effectiveness of SR in the case of dilation. Hence, we investigated the influence of flow separation on the effectiveness of SR in response to dilation.

In total there are 23 divergent bifurcations and 46 outflow branches in *network 2*. Every outflow branch at a divergent bifurcation was dilated, and the steady-state flow field was computed. Based on the steady-state results for the baseline case, the outflow branches are either balanced ($0.98 \leq |B_{db}| \leq 1.00$, 10 branches) or there is one branch with a smaller ($0.0 \leq -B_{db} < 0.98$, 18 branches) and one branch with a higher flow rate ($0 \leq B_{db} < 0.98$, 18 branches). At four divergent bifurcations the relative outflow rates differ drastically so that we do not expect the SR to be fully successful in the case of dilation.

To compare the effectiveness of SR between the different locations of dilation, the SR factor SR_{GenX} and the total SR factor SR_{tot} were introduced. The SR factor is the ratio between the relative flow change for simulations with and without RBCs:

$$SR_{GenX} = \frac{\Delta Q_{GenX}^{\text{with RBCs}}}{\Delta Q_{GenX}^{\text{no RBCs}}} \quad (20)$$

The total SR factor is calculated as the weighted sum of *generations 0–2* and is used to measure SR for the whole network in the case of dilation. As the relative flow change ΔQ_{Gen3} in *generation 3* is very small for all investigated scenarios, the SR factor for *generation 3* is not considered in the calculation of the total SR factor.

$$SR_{tot} = 0.6\ SR_{Gen0} + 0.3\ SR_{Gen1} + 0.1\ SR_{Gen2} \quad (21)$$

The weights for the different generations are chosen such that the impact of the dilated capillary is largest. Their sum is equal to 1.

SR is considered successful if $SR_{tot} \leq 0.7$. Our results show that SR works well for divergent bifurcations with similar outflow velocities. For comparatively well-balanced bifurcations ($0.90 \leq |B_{db}| < 0.98$) SR in the case of dilation is successful for the branch with the smaller outflow velocity. The effectiveness of SR decreases for ill-balanced divergent bifurcations. This means the RBCs are not able to fully compensate for the change in resistance introduced by capillary dilation. However, for all divergent bifurcations the resulting flow change in the dilated capillary was less for the simulation with RBCs.

Average values of SR_{GenX} for different generations are shown in Fig. 6 for different balance factors. It has to be emphasized that the values for *generation 2* have to be interpreted with caution. As mentioned above, the absolute changes for those generations are small, e.g., even for large SR_{Gen2} values the absolute changes are negligible.

In summary, SR in the case of dilation is effective in most (38/46) outflow branches of divergent bifurcations. The extent to which the RBCs are able to compensate for the induced changes depends on the flow situation at the bifurcation. The most important requirement for a successful SR is that bifurcations are well balanced and that a sufficient number of RBCs are present. An overall balanced network is beneficial to minimize changes induced by capillary dilations in the whole network. In equivalent studies with asymmetric hexagonal artificial networks similar results were obtained.

CONCLUSIONS AND DISCUSSION

In the presented work we analyzed the effects of capillary dilation on blood flow and RBC distribution and underlined the strong effects of RBCs on the network dynamics. For example, RBCs lead to balanced outflow rates at most diverging bifurcations. At such balanced bifurcations, we demonstrated that capillary dilation leads to an accumulation of RBCs and a reduced RBC velocity in the dilated capillary. This is in stark contrast to pure plasma flow and is a direct consequence of the bifurcation rule. While the RBCs accumulate in the dilated branch only, the flow rates do not change significantly. At less balanced divergent bifurcations equivalent effects were observed but were less pronounced. Moreover, the area of influence decreases for overall balanced networks. In summary, in ideal cases capillary dilation does not alter the blood flow, but increases the local RBC density. In the context of oxygen transport, a higher number of RBCs promoted by dilation is beneficial.

So far, our investigations are limited to artificial capillary networks but need to be extended to real ones. We showed that the success of SR mainly depends on the flow situation at diverging bifurcations. For most cases the changes induced by capillary dilations are very local. However, we observed that the area of influence of dilation increases in ill-balanced networks. It should be noted that the used symmetric hexagonal network is considerably smaller than realistic networks. Hence, to be able to comment in more detail on the area of influence of capillary dilation simulations should be executed in larger networks. Further research is needed to better understand the coupling between RBCs, balancing and SR in realistic networks.

For the symmetric hexagonal network we obtain the averaged balance factor for an inflow tube hematocrit of 0.25. This agrees well with the average values found in the rat cerebral cortex 0.24 ± 0.09 (27) and supports our hypothesis of well-balanced capillary networks. In further numerical simulations

Flow rates	Range
Balanced	$0.98 \leq \lvert B_{db}\rvert \leq 1.0$
Smaller	$0.90 \leq -B_{db} < 0.98$
Higher	$0.90 \leq B_{db} < 0.98$
Unbalanced	$\lvert B_{db}\rvert < 0.90$

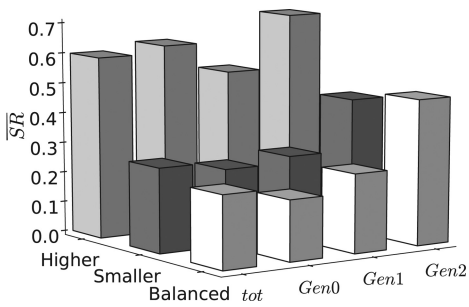

Fig. 6. The averaged self-regulation factor ($\overline{SR_{tot}}$, $\overline{SR_{Gen0}}$, $\overline{SR_{Gen1}}$, and $\overline{SR_{Gen2}}$) is displayed for different balance factors B_{db}.

Downloaded from journals.physiology.org/journal/ajpheart (192.041.132.005) on June 11, 2024.

the ideal tube hematocrit should be defined for realistic networks and compared with experimental data.

We focused on the changes resulting from dilations of single capillaries. However, most likely collective dilations and constrictions occur in realistic situations, which offers further opportunities for even more effective SR-related phenomena.

In the context of neurovascular coupling, we suggest that capillary dilation could be an important initial process taking place immediately after increases in neuronal activity and metabolic demand. Upon a consecutive arterial dilation the increased blood flow rate reaches the capillary bed only after capillary diameters have changed such that RBCs are distributed according to the higher cerebral metabolic rate of oxygen consumption (CMR_{O_2}).

Obviously, in vivo experiments are needed to confirm our results. However, such experiments are demanding, because ideally multiple locations in the capillary bed need to be measured to be able to compare the baseline to the dilated case.

The available experimental results mainly focus on the question whether capillary dilation contributes to increasing blood flow rates during neuronal stimulation (20, 36, 50). This differs fundamentally from our assumption, since we assume that capillary dilation influences the distribution of RBCs rather than the flow rate. Hence, the available experimental investigations are not fully suitable to validate our numerical observations. Fernandez-Klett et al. (20) indirectly support our assumptions as they concluded that capillary dilation can result in changes in RBC flow in single capillaries but that it plays a minor role in increasing the flow rate. Furthermore, in two reports capillary dilation and constriction was observed, which did not fit the expected pattern. This suggests that further, yet unknown, mechanisms may also lead to capillary dilation (20, 50). The influence of capillary dilation on RBC velocity and flow was also addressed in the work by Fernandez-Klett et al. (20). Unfortunately, they only measured values after arterial dilation therefore their results cannot be used to justify our simulations.

In the previous paragraphs we underlined the importance of overall well-balanced networks for the effectiveness of SR. It is evident that a well-balanced capillary network offers some advantages over an unbalanced network, e.g., that the RBC distribution is changed more easily. Experimental reports confirming this theory are, however, sparse. Only a few studies exist which monitor all capillaries connected to one divergent bifurcation. Tyml et al. (51) recorded the average RBC velocity in a capillary network with ≈50 capillaries of the frog's sartorius muscle. For 10 divergent bifurcations the RBC velocity of both outflow branches was measurable. Unfortunately, no information on the diameters of the individual vessels and on the tube hematocrit is available. Hence, we cannot compute the bulk flow velocity from the RBC velocity. As a first approach we compared the RBC velocity of the outflow branches, and for 8 out of 10 bifurcations the RBC velocities do not differ by more than 36%. In the work by Fraser et al. (21), various flow characteristics have been measured at eight microvascular divergent bifurcations of the rat's extensor digitorum longus muscle. Their results show that for six out of eight divergent bifurcations the bulk flow velocities differ by less than 34%. Recently, Landolt et al. (30) developed a new measuring technique to simultaneously measure the RBC velocity in all three branches of a divergent bifurcation. These data support our hypothesis on equalized bulk flow velocity in the outflow branches, but further measurements and simulations in realistic networks are needed to confirm our hypothesis.

It can be assumed that realistic capillary networks are built to promote well-balanced situations, and it was shown that hemodynamics may also play an important role in development (5, 6). Very illustrative proof was provided by Chen et al. (9). They followed the development of the midbrain of zebrafish in detail and were able to show that the created network is strongly influenced by blood flow. According to their results, vessel segments with very low flow rates are pruned and the overall flow distribution is equalized. This agrees well with our assumption that networks are built in a well-balanced fashion. However, the driving factors for developmental processes differ strongly between different organs and further investigations are needed to validate this hypothesis (5).

In summary, our work strongly underlines the large impact of RBCs on the dynamics in capillary networks. In the case of balanced capillary networks, dilation is a very efficient mechanism to locally increase the distribution of RBCs.

APPENDIX A: COMPARISON TO EMPIRICAL MODEL

To underline the significance of the discrete RBC tracking we compared our results with the frequently used iterative model based on empirical functions (24, 32, 33, 34, 42, 43, 47). The iterative empirical model is implemented as described in Secomb et al. (47) with the change that we used the more recent formulation to compute the phase separation and the effective resistance (41). The empirical model and the discrete model differ significantly in two aspects: *1*) the distribution of RBCs in the discrete model is directly obtained from the propagation of RBCs through the network. In the empirical model the distribution of RBCs is computed indirectly from the RBC fluxes at bifurcations. *2*) With the empirical model only steady-state results can be obtained. Transient effects and fluctuations in the RBC distributions cannot be analyzed.

In a first step we compared the results of the discrete and the empirical model for the dilated two-branch network (Fig. A1). Both models predict an increased number of RBCs n_{RBC} and a reduced RBC velocity u_{RBC} in the dilated branch. However, the increase in the number of RBCs as well as the decrease in the RBC velocity is more pronounced in the discrete model. In the empirical model the number of RBCs does not rise enough to compensate for the drop in resistance

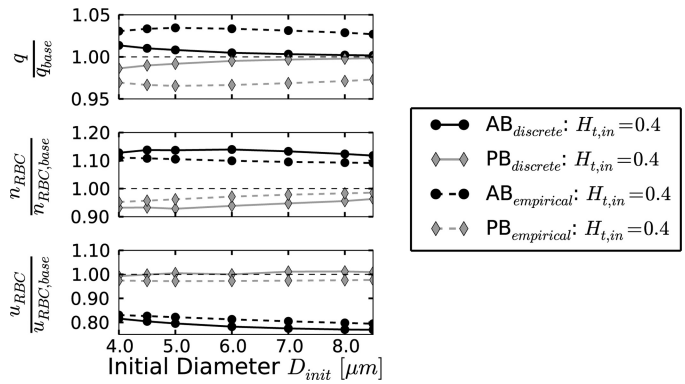

Fig. A1. Averaged flow rate, number of RBCs, and velocity of RBCs relative to baseline for different initial diameters (D_{init}) and different numerical models (discrete and empirical). Black lines illustrate the results in the AB and grey lines in the PB. The dilation factor is $f_{\mathrm{Dil}} = 15\%$. n_{RBC} is shown for the whole AB and PB, whereas u_{RBC} is the velocity in the dilated part of the AB and its undilated counterpart in the PB.

Downloaded from journals.physiology.org/journal/ajpheart (192.041.132.005) on June 11, 2024.

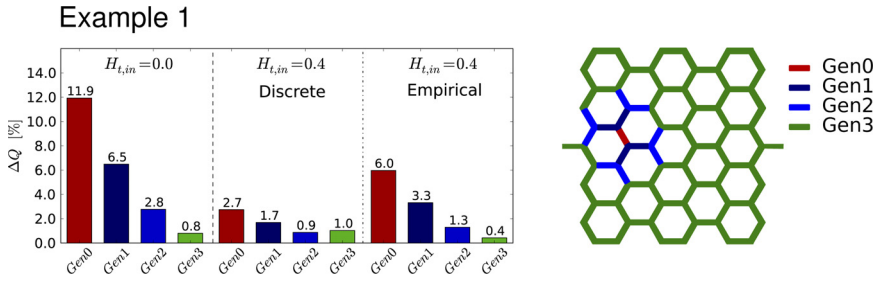

Fig. A2. Averaged relative flow change ΔQ_{GenX} for different generations in 1 example case. The results are compared for simulations without RBCs ($H_{t,in}$ = 0.0) and with $H_{t,in}$ = 0.4 for the discrete and the empirical model. The dilated capillary is highlighted in red in the schematic drawing of *network 2*. The dilation factor is f_{Dil} = 15%.

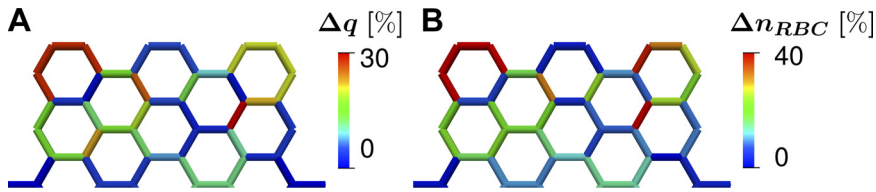

Fig. A3. Relative difference of the flow rate (Δq; *A*) and the number of RBC (Δn_{RBC}; *B*) between the discrete and the empirical model.

due to dilation and consequently the flow rate in the dilated branch is larger in the active branch.

In a second step we analyzed the relative flow change ΔQ_{GenX} in the hexagonal network for the dilation of the capillaries illustrated in Fig. 5, *A* and *B*. Figure A2 compares the results of the relative flow change for the discrete and the empirical model. Similar trends as in the two-branch network are observed. Compared with the simulation without RBCs the relative flow change is smaller for both numerical models. However, the SR effect is less pronounced in the empirical model. The number of RBCs n_{RBC} increases by 35.8% in the discrete model but only by 32.5% in the empirical model.

Already for the baseline case there are significant differences between the empirical and the discrete model. The relative difference in flow rate Δq and number of RBCs Δn_{RBC} is illustrated in Fig. A3. On average the flow rates differ by 16% and the number of RBCs by 24%. In summary, it can be stated that SR is observed with both numerical models but that the empirical model underestimates the effectiveness of SR.

ACKNOWLEDGMENTS

We thank Prof. A. Buck, Prof. D. Obrist, and A. Lücker for the constructive discussions and the valuable scientific input. We are also grateful for M. Barrett's comments on the manuscript and the feedback from the reviewers that further improved the manuscript.

GRANTS

Funding for this research was provided by the Swiss National Science Foundation Grant No. 140660.

DISCLOSURES

No conflicts of interest, financial or otherwise, are declared by the author(s).

AUTHOR CONTRIBUTIONS

Author contributions: F.S. performed experiments; F.S. analyzed data; F.S., B.W., and P.J. interpreted results of experiments; F.S. prepared figures; F.S. drafted manuscript; F.S., B.W., and P.J. edited and revised manuscript; J.R., B.W., and P.J. conception and design of research; B.W. and P.J. approved final version of manuscript.

REFERENCES

1. **Audet DM, OlbrichtWL.** The motion of model cells at capillary bifurcations. *Microvasc Res* 33: 377–396, 1987.
2. **Barber JO, Alberding JP, Restrepo JM, Secomb TW.** Simulated two dimensional red blood cell motion, deformation and partitioning in microvessel bifurcations. *Ann Biomed Eng* 36: 1690–1698, 2008.
3. **Baskurt OK, Farley RA, Meiselman HJ.** Erythrocyte aggregation tendency and cellular properties in horse, human, and rat. A comparative study. *Am J Physiol Heart Circ Physiol* 273: H2604–H2612, 1997.
4. **Blinder P, Tsao PS, Kaufhold JP, Knutsen PM, Suhl H, Kleinfeld D.** The cortical angiome: an interconnected vascular network with noncolumnar patterns of blood flow. *Nat Neurosci* 16: 889–897, 2013.
5. **Carmeliet P.** Mechanisms of angiogenesis and arteriogenesis. *Nat Med* 6: 389–395, 2000.
6. **Carmeliet P.** Angiogenesis in health and disease. *Nat Med* 9: 653–660, 2003.
7. **Carr RT, Geddes JB, Wu F.** Oscillations in a simple microvascular network. *Ann Biomed Eng* 33: 764–771, 2005.
8. **Carr RT, Lacoin M.** Nonlinear dynamics of microvascular blood flow. *Ann Biomed Eng* 28: 641–652, 2000.
9. **Chen Q, Jiang L, Li C, Hu D, Bu JW, Cai D, Du JL.** Haemodynamics-driven developmental pruning of brain vasculature in zebrafish. *PLoS Biol* 10: e1001374, 2012.
10. **Chien S, Tvetenstrand CD, Epstein MA, Schmid-Schoenbein GW.** Model studies on distribution of blood cells at microvascular bifurcations. *Am J Physiol Heart Circ Physiol* 248: H568–H576, 1985.
11. **Davis JM, Pozrikidis C.** Numerical simulation of unsteady blood flow through capillary networks. *Bull Math Biol* 73: 1857–1880, 2011.
12. **Dellimore JW, Dunlop MJ, Canham PB.** Ratio of cells and plasma in blood flowing past branches in small plastic channels. *Am J Physiol Heart Circ Physiol* 244: H635–H643, 1983.
13. **Ellis CG, Ellsworth ML, Pittman RN, BurgessWL.** Application of image analysis for evaluation of red blood cell dynamics in capillaries. *Microvasc Res* 44: 214–225, 1992.
14. **Ellis CG, Tyml K, Burgess WL.** Quantification of red cell movement in microvessels: a new application of interactive computer graphics. *Microvasc Res* 33: 428–32, 1987.
15. **Ellis CG, Wrigley SM, Groom AC.** Heterogeneity of red blood cell perfusion in capillary networks supplied by a single arteriole in resting skeletal muscle. *Circ Res* 75: 357–368, 1994.
16. **Ellsworth ML, Popel AS, Pittman RN.** Assessment and impact of heterogeneities of convective oxygen transport parameters in capillaries of striated muscle: experimental and theoretical. *Microvasc Res* 35: 341–362, 1988.
17. **Fåhraeus R.** The suspension stability of the blood. *Physiol Rev* 9: 241–274, 1929.
18. **Fåhraeus R, Lindqvist T.** The viscosity of blood flow in narrow capillary tubes. *Am J Physiol* 96: 562–568, 1931.
19. **Fenton BM, Wilson DW, Cokelet GR.** Analysis of the effects of measured white blood cell entrance times on hemodynamics in a compute model of a microvascular bed. *Pflügers Arch* 403: 396–401, 1985.
20. **Fernandez-Klett F, Offenhauser N, Dirnagl U, Priller J, Lindauer U.** Pericytes in capillaries are contractile in vivo but arterioles mediate functional hyperemia in the mouse brain. *Proc Natl Acad Sci USA* 107: 22290–22295, 2010.

Downloaded from journals.physiology.org/journal/ajpheart (192.041.132.005) on June 11, 2024.

21. **Fraser GM, Goldman D, Ellis CG.** Microvascular flow modeling using in vivo hemodynamic measurements in reconstructed 3D capillary networks. *Microcirculation* 6: 510–20, 2012.
22. **Fung YC.** Stochastic flow in capillary blood vessels. *Microvasc Res* 5: 34–48, 1972.
23. **Furman MB, Olbricht WL.** Unsteady cell distribution in capillary networks. *Biotechnol Prog* 1: 26–32, 1985.
24. **Guibert R, Fonta C, Plouraboue F.** Cerebral blood flow modeling in primate cortex. *J Cereb Blood Flow Metab* 30: 1860–1873, 2010.
25. **Hall CN, Reynell C, Gesslein B, Hamilton NB, Mishra A, Sutherland BA, O'Farrell FM, Buchan AM, Lauritzen M, Attwell D.** Capillary pericytes regulate cerebral blood flow in health and disease. *Nature* 508: 55–60, 2014.
26. **Hirsch S, Reichold J, Schneider M, Szekely G, Weber B.** Topology and hemodynamics of the cortical cerebrovascular system. *J Cereb Blood Flow Metab* 32: 952–967, 2012.
27. **Hudetz AG.** Blood flow in the cerebral capillary network: a review emphasizing observations with intravital microscopy. *Microcirculation* 4: 233–252, 1997.
28. **Kiani MF, Pries AR, Hsu LL, Sarelius IH, Cokelet GR.** Fluctuations in microvascular blood flow parameters caused by hemodynamic mechanisms. *Am J Physiol Heart Circ Physiol* 266: H1822–H1828, 1994.
29. **Klitzman B, Johnson PC.** Capillary network geometry and red cell distribution in hamster cremaster muscle. *Am J Physiol Heart Circ Physiol* 243: H211–H219, 1982.
30. **Landolt A, Obrist D, Wyss M, Barrett M, Langer D, Jolivet R, Soltysinksi T, Rösgen T, Weber B.** Tow-photon microscopy with double circle trajectories for in vivo cerebral blood flow measurements. *Exp Fluids* 54: 1523, 2013.
31. **Lipowsky HH, Usami S, Chien S.** In vivo measurements of apparent viscosity and microvessel hematocrit in the mesentery of the cat. *Microvasc Res* 19: 297- 319, 1980.
32. **Lorthois S, Cassot F, Lauwers F.** Simulation study of brain blood flow regulation by intra-cortical arterioles in an anatomically accurate large human vascular network: Part I: Methodology and baseline flow. *Neuroimage* 54: 1031–1042, 2001.
33. **Lorthois S, Cassot F, Lauwers F.** Simulation study of brain blood flow regulation by intra-cortical arterioles in an atomically accurate large human vascular network: Part II: Flow variations induced by global or localized modifications of arteriolar diameters. *Neuroimage* 54: 2840–2853, 2011.
34. **Lorthois S, Lauwers F.** Control of brain blood flow by capillaries: a simulation study in an anatomically accurate large human vascular network. *Comput Methods Biomech Biomed Engin* 15: 66–68, 2012.
35. **Obrist D, Weber B, Buck A, Jenny P.** Red blood cell distribution in simplified capillary networks. *Philos Trans A Math Phys Eng Sci* 368: 2897–2918, 2010.
36. **Peppiatt CM, Howarth C, Mobbs P, Attwell D.** Bidirectional control of CNS capillary diameter by pericytes. *Nature* 443: 700–704, 2006.
37. **Pop SR, Richardson G, Waters SL, Jensen OE.** Shock formation and nonlinear dispersion in a microvascular capillary network. *Math Med Biol* 24: 379–400, 2007.
38. **Pozrikidis C.** Numerical simulation of blood flow through microvascular capillary networks. *Bull Math Biol* 71: 1520–1541, 2009.
39. **Pries AR, Ley K, Claassen M, Gaehtgens P.** Red cell distribution at microvascular bifurcations. *Microvasc Res* 38: 81–101, 1989.
40. **Pries AR, Neuhaus D, Gaehtgens P.** Blood viscosity in tube flow: dependence on diameter and hematocrit. *Am J Physiol Heart Circ Physiol* 263: H1770–H1778, 1992.
41. **Pries AR, Secomb TW.** Microvascular blood viscosity in vivo and the endothelial surface layer. *Am J Physiol Heart Circ Physiol* 289: H2657–H2664, 2005.
42. **Pries AR, Secomb TW, Gaehtgens P.** Relationship between structural and hemodynamic heterogeneity in microvascular networks. *Am J Physiol Heart Circ Physiol* 270: H545–H553, 1996.
43. **Pries AR, Secomb TW, Gaehtgens P, Gross JF.** Blood flow in microvascular networks experiments and simulation. *Circ Res* 67: 826–834, 1990.
44. **Reichold J, Stampanoni M, Keller AL, Buck A, Jenny P, Weber B.** Vascular graph model to simulate the cerebral blood flow in realistic vascular networks. *J Cereb Blood Flow Metab* 29: 1429–1443, 2009.
45. **Schmid-Schönbein GW, Skalak R, Usami S, Chien S.** Cell distribution in capillary networks. *Microvasc Res* 19: 18–44, 1980.
46. **Schulte ML, Wood JD, Hudetz AG.** Cortical electrical stimulation alters erythrocyte perfusion pattern in the cerebral capillary network of the rat. *Brain Res* 963: 81–92, 2003.
47. **Secomb TW, Pries AR, Gaehtgens P, Gross JF.** Theoretical and experimental analysis of hematocrit distribution in microcirculatory networks. In: *Microvascular Mechanics: Hemodynamics and Systemic and Pulmonary Microcirculation*. New York: Springer-Verlag, 1989, p. 39–49.
48. **Secomb TW, Styp-Rekowska B, Pries AR.** Two-dimensional simulation of red blood cell deformation and lateral migration in microvessels. *Ann Biomed Eng* 35: 755–765, 2007.
49. **Sessoms DA, Amon A, Courbin L, Panizza P.** Complex dynamics of droplet traffic in a bifurcation microfluidic channel: periodicity, multistability, and selection rules. *Phys Rev Lett* 105: 154501, 2010.
50. **Stefanovic B, Hutchinson E, Yakovleva V, Schram V, Russell JT, Belluscio L, Koretsky AP, Silva AC.** Functional reactivity of cerebral capillaries. *J Cereb Blood Flow Metab* 28: 961–972, 2008.
51. **Tyml K, Ellis CG, Safranyos RG, Fraser S, Groom AC.** Temporal and spatial distributions of red cell velocity in capillaries of resting skeletal muscle, including estimates of red cell transit times. *Microvasc Res* 22: 14–31, 1981.
52. **Villringer A, Them A, Lindauer U, Einhäupl K, Dirnagl U.** Capillary perfusion of the rat brain cortex an in vivo confocal microscopy study. *Circ Res* 75: 55–62, 1994.
53. **Yen RT, Fung YC.** Effect of velocity distribution on red cell distribution in capillary blood vessels. *Am J Physiol Heart Circ Physiol* 235: H251–H257, 1978.

Downloaded from journals.physiology.org/journal/ajpheart (192.041.132.005) on June 11, 2024.